Inorganic Chemistry

Article

pubs.acs.org/IC

Structure and Spectroscopic Properties of Gold(I) Diselenophosph(in)ate Complexes: A Joint Experimental and Theoretical Study

Camille Latouche,[†] Yu-Chen Lee,[‡] Jian-Hong Liao,[‡] Eric Furet,[†] Jean-Yves Saillard,*[,†] C. W. Liu,*[,‡] and Abdou Boucekkine*[,†]

[†]Institut des Sciences Chimiques de Rennes, UMR 6226 CNRS-Université de Rennes 1, Campus de Beaulieu, 35042 Rennes cedex, France

[‡]Department of Chemistry, National Dong Hwa University, Hualien, Taiwan 97401, Republic of China

Supporting Information

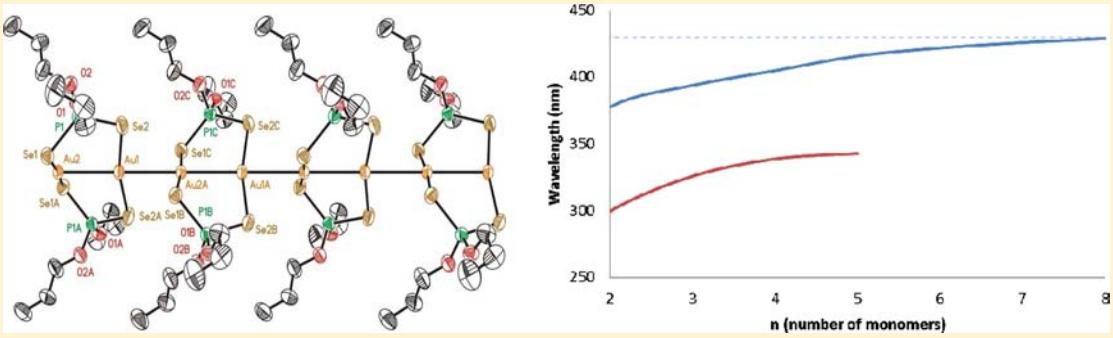

ABSTRACT: The structure and optical properties of several polynuclear gold(I) species, namely, diselenophosphate $[Au\{\mu\text{-}Se_2P(OR)_2\}]_2$ complexes (R = ^{i}Pr, Et, ^{n}Pr) respectively numbered **1**, **2**, and **3** and number **4** $[Au\{\mu\text{-}Se_2P(CH_2)_2Ph)_2\}]_2$, exhibiting interesting structural, absorption, and emission properties have been studied. The synthesis, full characterization, and experimental spectroscopic study of **3** and **4** have first been carried out, **1** and **2** being previously studied. In the solid state, **3** gives polymers, like **1** and **2**, whereas **4** exists under a dinuclear monomeric form. The absorption and phosphorescence properties of **4** have been rationalized using DFT and TDDFT computations. In particular, Au−Au bonding seems to appear in its first singlet and triplet states, whereas such a bond does not exist in the ground state. Then, the influence of polymerization through aurophilic bonding on the optical properties of **2** is investigated (**1** and **3** behave as **2**). It is shown using TDDFT computations that its observed UV−visible excitation spectrum in solution is due to high oligomers and not to monomers or low size oligomers. ESI-MS molecular weight measurements confirm the occurrence of such oligomers of **2** in solution. An assignment of the observed bands of **2** is proposed. The transition corresponding to the first excitation band, which is mainly a HOMO to LUMO one, exhibits metal-centered character, i.e., a gold 5d to 6p orbital transition, but concomitantly transfers significant electron density from gold to phosphorus atoms so that it is also a MLCT one.

1. INTRODUCTION

Polynuclear Au(I) compounds exhibit a very large domain of applications[1] such as the design of electronic, sensor, and luminescence devices or photocatalysis and also biology. Some of them appear as polymers, exhibiting Au···Au bonding due to the so-called aurophilic interaction.[2] This interaction has been largely studied and reviewed in particular by Pyykkö.[3]

In the present paper, we intend to investigate a series of diselenophosph(in)ate $[Au\{\mu\text{-}Se_2P(OR)_2\}]_2$ (**1**, R = ^{i}Pr; **2**, R = Et; and **3**, R = ^{n}Pr) species and **4** $[Au\{\mu\text{-}Se_2P(CH_2)_2Ph)_2\}]_2$ (Scheme 1), with a focus on the influence of the ligands and oligomerization on their structural and spectroscopic properties. Previous theoretical studies of dinuclear gold(I) complexes are found in the literature,[4] recent review articles are available,[1a,b] generally focusing on structural aspects or luminescence properties of monomers, dimers or trimers. It is worth noting the experimental and theoretical investigation of excited state interactions of $[Au(CN)_2^-]_n$ oligomers in solution.[5]

In this paper, in addition to **1** and **2**, which have been previously synthesized and fully characterized[6] by some of us, we describe first the synthesis and structural characterization of complexes **3** and **4**, as well as their absorption and emission properties.

The computational study which follows, using different quantum mechanical methods, namely Density Functional Theory (DFT), Moller−Plesset second order perturbation

Received: August 11, 2012
Published: October 25, 2012

   dx.doi.org/10.1021/ic301763k | *Inorg. Chem.* 2012, 51, 11851−11859

Scheme 1

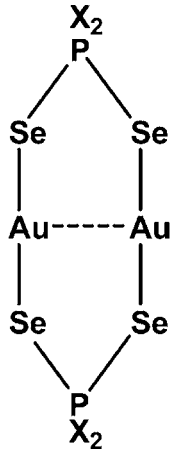

1: X = O^{i}Pr
2: X = OEt
3: X = O^{n}Pr
4: X = P(CH$_2$)$_2$Ph

theory (MP2; a post-Hartree−Fock method), and time dependent DFT (TDDFT), should allow us to describe the electronic structure of the species under consideration and to assign their electronic and emission spectra.

2. EXPERIMENTAL SECTION

2.1. Synthesis, Characterizations, and Spectra. All chemicals were of analytical grade, available commercially, and used as received. Solvents were purified following standard procedures.[7] Standard Schlenk techniques were employed for performing all reactions under an inert atmosphere. The ligands, $NH_4Se_2P(OPr)_2$ and $NH_4[Se_2P\{(CH_2)_2Ph\}_2]$,[8] were prepared according to the literature methods. The elemental analyses were done using a Perkin-Elmer 2400 CHN analyzer. ^{1}H, ^{31}P, and ^{77}Se NMR spectra were recorded on an Advance-300 Fourier transform spectrometer. H_3PO_4 (δ = 0) and PhSeSePh (δ = 463) were used as the external reference for ^{31}P and ^{77}Se NMR, respectively. UV−visible absorption spectra were recorded on a HP 8453 photodiode array spectrometer. Emission spectra were recorded on a Cary Eclipse B10 fluorescence spectrophotometer. Emission spectra were corrected for instrumental responses.

Synthesis of [Au{μ-Se$_2$P(O^{n}Pr)$_2$}]$_2$ (3). A mixture of $NH_4[Se_2P(O^nPr)_2]$ (0.034 g, 0.094 mmol) and AuCl(tht) (0.094 mmol) was stirred in 30 mL of THF at −50 °C under a nitrogen atmosphere for 4 h. The slight yellow solution obtained was filtered and dried in a vacuum. The residue was washed with deionized water and dried under a vacuum to obtain a yellow powder. The resultant yellow powders were recrystallized from diethyl ether at −20 °C. Yield: 0.035 g (74%). ^{1}H NMR (300 MHz, $CDCl_3$; δ, ppm): 1.03 (t, $^3J_{HH}$ = 7.4 Hz, 12H, $OCH_2CH_2CH_3$), 1.82 (m, 8H, $OCH_2CH_2CH_3$), 4.23 (m, 8H, $OCH_2CH_2CH_3$). ^{31}P{^{1}H} NMR (121.49 M Hz, $CDCl_3$; δ, ppm): 67.73 (J_{P-Se} = 632 Hz). ^{77}Se NMR(57.24 MHz, $CDCl_3$; δ, ppm): 309.5(d, J_{P-Se} = 632 Hz). IR [CsI, ν(Au−Se)]: 236 cm^{-1}. mp: 112 °C. Anal. Calcd for $C_{12}H_{28}Au_2O_4P_2Se_4{\cdot}0.4C_4H_8O$: C, 15.75; H, 3.03. Found: C, 15.60; H, 3.26.

Synthesis of [Au{μ-Se$_2$P{(CH$_2$)$_2$Ph}$_2$}]$_2$ (4). Compound **4** was synthesized in a similar procedure to **3** using $NH_4[Se_2P\{(CH_2)_2Ph\}_2]$ (0.034 g, 0.078 mmol) instead of $NH_4[Se_2P(O^nPr)_2]$. Yield: 0.028 g (60.2%). ^{1}H NMR (300 MHz, $CDCl_3$, δ, ppm): 2.75 (m, 8H, CH_2Ph), 3.14 (m, 8H, PCH_2), 7.22(m, 20H, *Ph*). ^{31}P{^{1}H} NMR (121.49 M Hz,$CDCl_3$, δ, ppm): 29.55 (J_{P-Se} = 495.8 Hz). ^{77}Se NMR(57.24 MHz, $CDCl_3$, δ, ppm): 198.7 (d, J_{P-Se} = 496.1 Hz). IR [CsI, ν(Au−Se)]: 245 cm^{-1}. mp: 169 °C. Anal. Calcd for $C_{32}H_{36}Au_2P_2Se_4{\cdot}3H_2O$: C, 30.84; H, 3.40. Found: C, 30.92; H, 3.54.

Crystal Data for 3 (CIF File in the SI). $C_{12}H_{28}Au_2O_2P_2Se_4$, M = 1008.06, orthorhombic, *Pccn*, a = 8.8851(11) Å, b = 23.393(3) Å, c = 12.0871(15) Å, V = 2512.3(6) Å^3, Z = 4, ρ_{calcd} = 2.665 g/cm^3, μ = 17.60 mm^{-1}, 2399 reflections collected, 1592 unique (R_{int} = 0.041), which were used in all calculations. Final R_1 [$I > 2\sigma(I)$] was 0.0347, and wR_2 (for all data) was 0.1133. GoF = 1.016. Max/min: 1.246/−0.966 e A^{-3}.

Crystal Data for 4 (CIF File in the SI). $C_{32}H_{36}Au_2P_2Se_4$, M = 1192.32, triclinic, $P(-)1$, a = 9.7733(8) Å, b = 13.1376(11) Å, c = 14.1643(12) Å, α = 79.489(2), β = 84.857(2), γ = 72.986(2), V = 1708.6(2) Å^3, Z = 2, ρ_{calcd} = 2.318 g/cm^3, μ = 12.95 mm^{-1}, 6044 reflections collected, 4892 unique (R_{int} = 0.038), which were used in all calculations. Final R_1 [$I > 2\sigma(I)$] was 0.0260 and wR_2 (for all data) was 0.0603. GoF = 1.026. Max/min: 1.332/−0.750 e A^{-3}. CCDC reference numbers: 796 842 for **3**; 875 038 for **4**. Data were collected at 296 K on a Bruker APEX-II CCD diffractometer. The unit cell parameters were calculated and refined from the full data set. The SMART software[9] was used for data acquisition, and the SAINT-Plus[10] software was used for data reduction. The absorption corrections were performed with the help of the SADABS program.[11] The structure was solved by direct methods and refined by full-matrix least-squares on F^2 using the SHELXTL software package incorporated in *SHELXTL*, PC version 5.10.[12] Selected bond distances and angles of **3** and **4** are listed in Table 1.

Table 1. Selected Bond Lengths (Å) and Angles (deg) of Complexes 3 and 4

intramolecular	3	4
Au−Au	2.9910(7)	3.387, 3.456
Au−Se	2.389(1)	2.387(1)
	−2.407(1)	−2.397(1)
Se−P	2.160(3)	2.174(2)
	−2.175(3)	−2.184(2)
Se−Au−Se	164.95(5)	171.98(2)
	−174.26(5)	−172.79(2)
Se−P−Se	119.80(11)	116.69(7)
	−119.80(11)	−118.76(7)
Se−Au−Au−Se	142.62(4)	180
intermolecular	3	4
Au−Au	3.0526(7)	3.485(4)
Au−Au−Au	180	

2.2. Computational Details. At the DFT level of theory, several functionals and basis sets were tested (results are given in the SI). After benchmarking (results in SI), the PBE0 hybrid functional[13] was chosen together with the LanL2DZ basis set[14] augmented with polarizations functions on all atoms, except hydrogen ones. A diffuse "d" orbital (exponent equal to 0.02) was been added on gold atoms. The optimized geometries of the dinuclear species were characterized as true minima on the potential energy surface using vibrational frequency calculations. Then, TDDFT calculations were performed on all species under consideration using either their optimized geometries or geometries generated from their X-ray structures, in order to compute their electronic spectra. Unless specified, computations took into account the solvent effects (THF), using the PCM model.[15] The program used for the DFT and TDDFT computations was Gaussian 09.[16] Representations of molecular structures and orbitals were done using the Molekel program,[17] and the orbital compositions were obtained using the AOMix program.[18]

We first studied computationally [Au{μ-Se$_2$P(CH$_2$)$_2$Ph)$_2$}]$_2$ (**4**) and [Au{μ-Se$_2$P(OEt)$_2$}]$_2$ (**2**). In the latter case, we considered the "monomeric species," i.e., the dinuclear complex [Au{μ-Se$_2$P(OEt)$_2$}]$_2$ that we call [Au]$_2$, as well as its [Au]$_{2n}$ oligomers with n = 2−8, in order to study the effect of the chain lengthening on the investigated properties. According to the very long computer time needed to simulate the electronic spectra of the largest oligomers, only few excitations have been computed for these species, allowing us to estimate the largest wavelength excitation only.

Geometry optimizations have also been carried out at the MP2 level of theory with the same program and basis set as for DFT calculations, but for [Au]$_2$ and [Au]$_4$ only, due to the computational time limitations.

3. RESULTS AND DISCUSSION

3.1. Structural and Spectroscopic Results. Structurally characterized dinuclear gold(I) complexes in which each gold(I) center is digonally coordinated by two Se atoms have been observed in two types of molecules: three connected by polyselenides such as $[Au_2(Se_2)(Se_4)]^{2-}$,[19] $[Au_2(Se_2)(Se_3)]^{2-}$,[19] and $[Au_2(Se_2Te)_2]^{2-}$,[20] and two by diselenophosphates, $[Au\{\mu\text{-}Se_2P(OR)_2\}]_2$ (R = ^{i}Pr, **1**; Et, **2**).[6] The latter molecules display intriguing concentration-dependent emission properties probably originating from different aggregate sizes with various degrees of aurophilically linked oligomers. In order to correlate the degrees of aggregation with the luminescent origin, the studies of absorption spectroscopies recorded in various concentrations were undertaken. Whereas the UV−vis spectra did not provide the informative data needed, the excitation spectra of both **1** and **2** in 2-MeTHF at 77 K do display bathochromic shifts as the concentration increases (Table 2), which is consistent with some molecular aggregations to become oligomers taking place.[6] These results encouraged us to prepare more derivatives with the aim that similar excitation characteristics can be uncovered. Herein, two Se-donor ligands are used: one is the propyl derivative of diselenophosphates, and the other is the selenoorganophosphorus unit, namely, diethylphenyl diselenophosphinate.

Table 2. Photophysical Data for Complexes 1∼4 at 77 K

compound	medium	λ_{max}^{ex}, nm	λ_{max}^{em}, nm
1(^{i}**Pr**)	solid	470	579
	glass[a]	294, 311 (3.3×10^{-5} M)	464
		341, 412 (5.4×10^{-4} M)	509, 540
		440 (3.3×10^{-3} M)	500, 540, 625
2(**Et**)	solid	388, 467	575
	glass[a]	350 (2.0×10^{-5} M)	630
		361, 390 (4.0×10^{-4} M)	650
		361, 418 (7.4×10^{-3} M)	650
3(**Pr**)	solid	414, 459	566
	glass[a]	356, 412 (4.7×10^{-5} M)	628
		351, 423 (5.7×10^{-3} M)	636
4	solid	434	593
	glass[a]	365 (6.3×10^{-5} M)	560
		389 (6.6×10^{-4} M)	560
		402 (5.2×10^{-3} M)	558

[a]Measured in 2-MeTHF.

Homoleptic, dinuclear gold(I) compounds **3** and **4** can be easily synthesized via the reaction of a stoichiometric amount of Au(tht)Cl with Se-donor ligands in THF at −50 °C. Both compounds were fully characterized by multinuclear solution NMR spectroscopies and their compositions by elemental analyses. A typical singlet peak with a set of selenium satellites is identified from the ^{31}P NMR spectrum (67.73 ppm, J_{P-Se} = 632 Hz for **3** and 29.55 ppm, J_{P-Se} = 495.8 Hz for **4**). This coupling constant is in good agreement with that revealed in the ^{77}Se NMR spectrum, 309.5 ppm (d, J_{P-Se} = 632 Hz) for **3** and 198.7 ppm (d, J_{P-Se} = 496.1 Hz) for **4**. ^{1}H NMR spectra of **3** and **4** display a set of chemical shifts corresponding to the resonance frequency of propyl and phenylethyl groups, respectively. In addition, the ν(Au−Se) stretching is recorded at 236 and 245 cm^{-1} for **3** and **4**, respectively, by using a CsI pellet. These numbers are consistent with the reported absorption at 236 cm^{-1} from $[Au_2(Se_2)(Se_4)]^{2-}$ and $[Au_2(Se_2)(Se_3)]^{2-}$.[19] Finally compounds **1**−**4** are not very stable at ambient temperature and must be kept in the freezer in an inert atmosphere.

Shown in Figure 1 is the packing diagram of the X-ray structure of **3**, which displays a one-dimensional linear chain

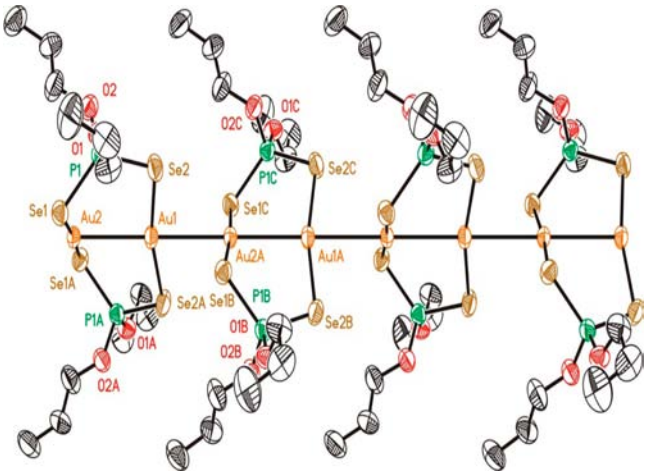

Figure 1. A thermal ellipsoid drawing of the X-ray structure of **3** displaying a 1D chain.

built by a repeating digold(I) unit bridged by two dipropyl diselenophosphates. It appears to be iso-structural with the ethyl analogue. Both intra- and intermolecular Au−Au distances (2.9910(7), 3.0526(7) Å) are comparable with 2.9434(9) and 3.0325(9) Å found in $[Au\{\mu\text{-}Se_2P(OEt)_2\}]_2$, **2**.[6] While the Au−Se bond lengths, 2.389(1)∼2.407(1) Å, are normal to the ethyl derivative,[6] the torsion angle of a puckered eight-membered ring, a metallocycle formed by two gold atoms and two PSe_2 units, is 142.62°, significantly larger than 136.08° revealed in **2**. Similarly, the Se−Au−Se angles, ranging from 164.95(5) to 174.26(5)°, indicate nonperfect linearity.

On the other hand, much longer Au···Au distances, 3.387 and 3.456 (intra) and 3.485 Å (inter), are observed in the X-ray structure of **4** (Figure 2), in which the digold(I) unit is bridged by two organoselenophosphorus moieties, the first of its kind. Intriguingly, the characteristic aurophilic interactions generally demonstrated in compounds **1**−**3** to form a linear chain appear not so important in **4** so that only a discrete dinuclear unit is yielded. The steric hindrance arising from the free rotation of phenylethyl groups obviously has a profound influence on the molecular packing. In addition, the puckered eight-membered ring observed in **3** relaxes back to a chair conformation in **4** of which the torsion angle of Se−Au−Au−Se is 180°. Aside from these points, the metric data of **4** are very similar to those of **3** (Table 2).

Compound **3** displays an orange emission (λ^{em}_{max} = 566 nm) in the solid state and red color (λ^{em}_{max} = 636 nm) in 2-MeTHF glass at 77 K (table 2). The excitation spectrum in the solid state shows a broad band between 380 and 490 nm and a maximum at 459 nm. It is noted that there is no absorption in dilute solution extending over 380 nm. While almost no shift in the emission wavelength in a glassy state upon the concentration increases from 4.7×10^{-5} M to 5.7×10^{-3} M, the excitation spectrum does barely red-shift to 423 nm, which suggests molecular aggregates already existing at 77 K at concentrations as low as 4.7×10^{-5} M. Overall both excitation and emission spectra of **3** show great resemblance to the ethyl

dx.doi.org/10.1021/ic301763k | Inorg. Chem. 2012, 51, 11851−11859

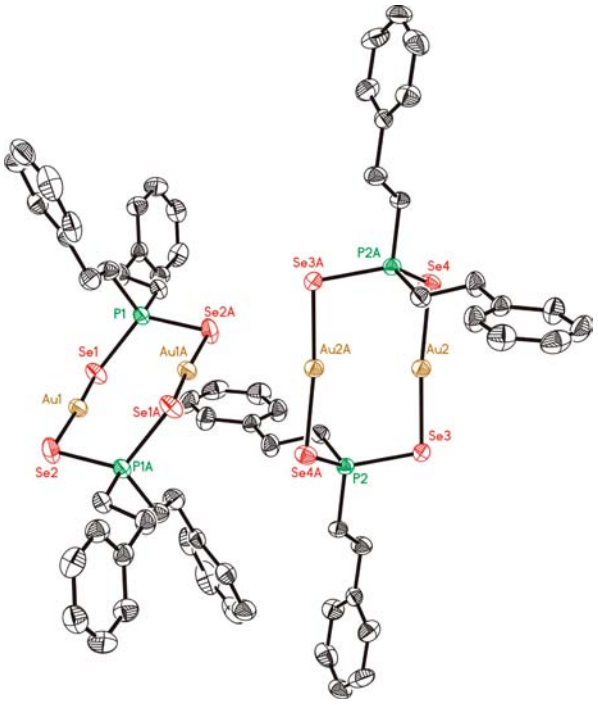

Figure 2. A thermal ellipsoid drawing showing a perspective view of the X-ray structure of **4**.

derivative, **2**. Indeed, their similarity in luminescent behavior is primarily due to the nearly identical solid state structure.

Two structureless bands, each centered at 434 and 593 nm, are displayed in the excitation and emission spectra of **4**, respectively, in the solid state at 77 K (table 2). The emission maximum shows a slight hypsochromic shift to 560 nm in solution at 77 K. Surprisingly, the excitation spectrum in 2-MeTHF at 77 K displays a bathochromic shift from 365 to 402 nm upon the increase in concentration from 6.3×10^{-5} M to 5.2×10^{-3} M (Figure 3). Considering the lack of aurophilic interactions revealed from the solid state structure, the concentration-dependent excitation in 2-MeTHF glass at 77 K strongly suggests that the distortions due to the molecular aggregations to form oligomers occur in the excited state. Indeed, as it will be seen later, thanks to DFT and TDDFT computations, such a possibility is credible.

3.2. Computational Results. *[Au{μ-$Se_2P\{(CH_2)_2Ph\}_2$}]$_2$* (***4***). We start the analysis considering complex **4**, which is of C_i symmetry and which exists as independent dinuclear monomers in the solid state. Its optimized geometry is shown in Figure 4 (left) with the atom labeling used in the following discussion. In Table 3, relevant geometrical values computed at different levels of theory are compared to the averaged X-ray ones.

As it can be seen, a rather good agreement is obtained between the DFT distances and angles and the X-ray data, especially the long Au···Au distance which, as expected, is reasonably well reproduced computationally, since no strong aurophilic interaction seems to occur for this species. On the contrary, it is worth noting that the MP2 Au···Au distance is significantly shorter than the X-ray one. The MP2 underestimation of such Au···Au distances using MP2 calculation has already been described.[3b] Finally, at such an observed Au···Au internuclear distance, no bonding is expected between gold atoms; the NBO analysis that we carried out at the DFT level does not reveal any Au−Au bonding MO.

We consider now the observed excitation spectra of **4**. The computed absorption wavelength is equal to 359 nm (oscillator strength $f = 0.006$), with the THF solvent taken into account, which compares very well with the observed value, 365 nm for the most dilute solution (6.3×10^{-5} M concentration). The corresponding transition is mainly a HOMO to LUMO one (percentage weight = 94%). Absorption at shorter wavelengths is computed at *ca.* 260−270 nm, but the domain range of the measured excitation is only 280−500 nm, so that no comparison with experimental results could be done. In order to investigate the nature of the HOMO−LUMO transition, we consider first the frontier MO diagram of complex **4** (Figure 5). In this figure are given the percentage contributions of gold atom and gold atomic orbitals as well as the selenium- and phosphorus-atom and hydrocarbon-group (noted CH) contributions to the MOs.

As can be seen, the HOMO is mainly constituted of selenium lone pairs, mixed with what can be in first approximation described as an out of phase combination of $5d_{z^2}$ gold orbitals (considering the z axis perpendicular to the Au−Au and Se−

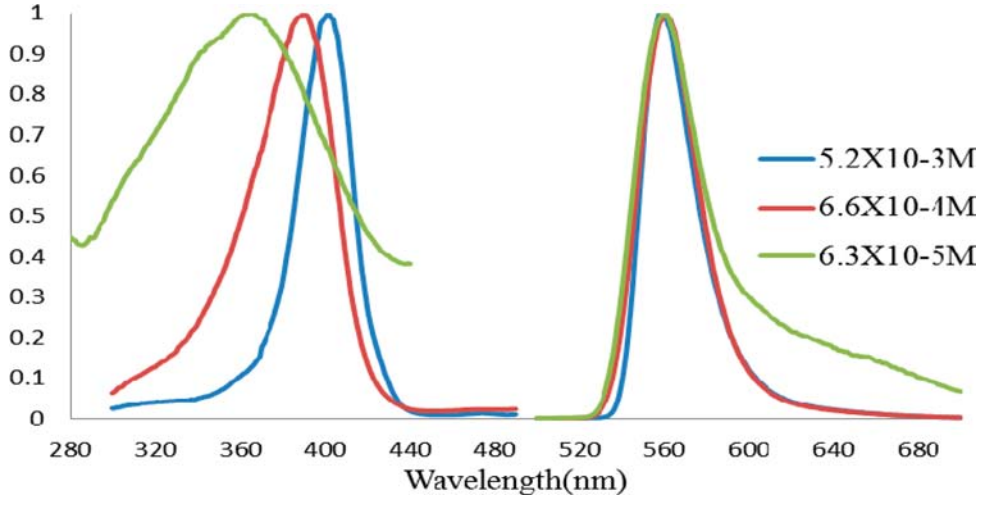

Figure 3. Normalized excitation and emission spectra of **4** in 2-MeTHF glass at 77 K under different concentrations.

dx.doi.org/10.1021/ic301763k | *Inorg. Chem.* 2012, 51, 11851−11859

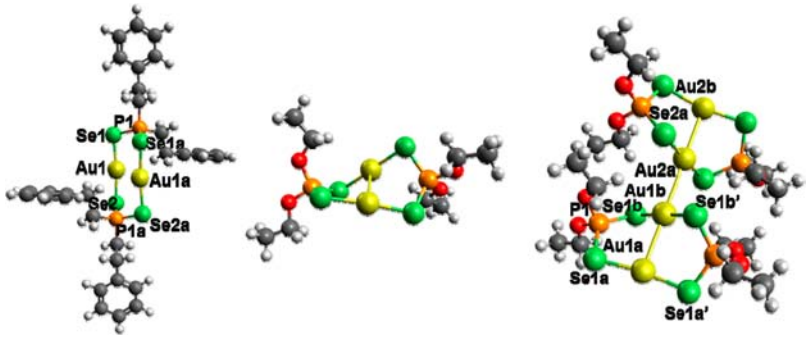

Figure 4. DFT optimized geometries of **4** (left) and of **2** in its monomeric form $[Au]_2$ (middle) and dimeric form $[Au]_4$ (right).

Table 3. Computed and Averaged X-Ray Metrical Data of Complex 4 (See Figure 4 for Atom Labeling; Distances are in Ångstroms and Angles in Degrees)

		DFT/PBE0 ground state		TDDFT/PBE0 (THF) first excited states			
geometrical parameter	X-ray	vacuum	THF	singlet	triplet	MP2 ground state	MP2 first excited triplet state
Au1−Au1a	3.442	3.381	3.350	2.752	2.691	3.093	2.696
Au1a−Se1a	2.392	2.459	2.461	2.485	2.514	2.458	2.486
Se1−P1	2.178	2.221	2.229	2.265	2.250	2.209	2.229
Se1a−Au1a−Se2a	172	170	170	155	155	164	154
Se1−P1−Se2a	118	118	116	116	115	117	117
Se1−Au1−Au1a−Se2a	180	180	180	180	180	180	180

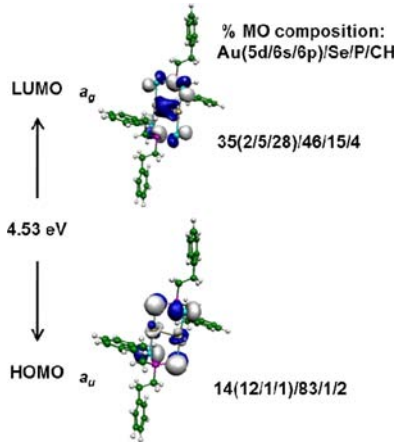

Figure 5. Plots (cutoff equal to 0.035 au) and compositions of the HOMO and LUMO of complex **4** (C_i symmetry).

Au−Se vectors). Indeed, the five 5d Au(I) orbitals are occupied, and the highest 5d-type combination of $[Au]_2$ is the antibonding combination of the d_{z^2} AOs. Since the 5d (Au) lie not far below in energy from the Se lone pairs, they mix, giving rise to the current selenium-based HOMO. The LUMO is of different origin. Since the 14-electron gold atoms are approximately linearly dicoordinated, their sp hybridization along the Se−Au−Se axis leaves two nonbonding vacant 6p orbitals on each metal, perpendicular to this axis. In the dinuclear unit, the 6p orbitals (along the Au−Au axis) overlap in a σ-type fashion so that their bonding combination becomes the LUMO after important mixing with an orbital which is both Au−Se and Se−P antibonding and which lies in the same energy range. This antibonding orbital has significant, although not dominant, 6s character. The mixing on this latter (6s-containing) orbital with the 6p bonding combination is roughly sketched in Scheme 2. It tends to somehow the lowest (6p-type) in a way which reinforces its intramolecular Au−Au bonding character, whereas the highest (6s-containing) has its electron density somehow pushed away from the Au−Au vector, making this orbital well suited to overlapping with congeners from neighboring dinuclear units aligned on the Au−Au axis (see Scheme 2). Such a polymeric situation does not occur in the case of compound **4**, but the role played by the vacant 6s-containing one will be discussed later when considering oligomerization of compound **2**.

Scheme 2

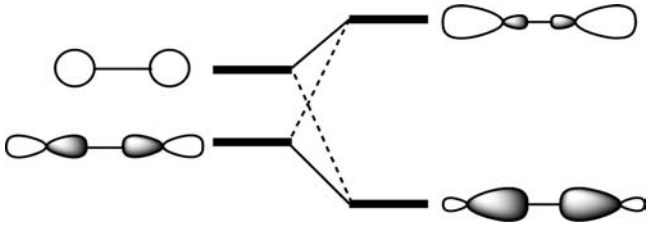

Back to **4**, the selenium weight decreases drastically when going from the HOMO (83%) to the LUMO (46%). Consequently, the HOMO−LUMO transition transfers electron density from the selenium atoms to the phosphorus atoms with a small amount, but more importantly to the gold atoms and particularly to their 6p orbitals. A 5d to 6p gold-centered electron transfer also occurs, the weight of the 5d orbitals decreasing from 12% in HOMO to 2% in LUMO.

We considerer now the first singlet and triplet excited states of **4**. Optimizations of the excited state geometries have been carried out using TDDFT computations at the same DFT level of theory. The latter ones are compared to the ground state geometry in Table 3. The most striking result is that the relaxed excited geometries exhibit very short Au−Au distances, 2.752 Å and 2.691 Å for the singlet and triplet state, respectively. The MP2 geometry optimization of the first triplet state leads to the same short Au−Au distance (2.697 Å). It must be noted that

dx.doi.org/10.1021/ic301763k | *Inorg. Chem.* 2012, 51, 11851−11859

such a shortening upon excitation to the first triplet state of the Au···Au distance by roughly 0.5 Å has also been obtained by DFT calculations on dinuclear N-heterocyclic dicarbene gold(I) complexes of general formula $[Au_2(RIm\text{-}Y\text{-}ImR)_2](PF_6)_2$ (R = Me, Cy; Y = $(CH_2)_{1-4}$, oxylylene, *m*-xylylene).[21a] Such possible shortening of the Au···Au distance in the excited state was already suggested by Fackler's group[21b] in 1989. This short Au−Au distance is related to the strong Au−Au σ-bonding character of the LUMO (Figure 5) and is indicative of the occurrence of a bond between the two atoms. This is confirmed by the NBO analysis carried out for the first triplet state. Indeed, a bonding Au···Au MO between gold hybrid orbitals, which does not exist in the ground state, is revealed by the computations, the composition of the latter hybrid orbitals being d (6%), s (86%), and p (8%).

The TDDFT computed emission wavelength from the first triplet excited state is equal to 495 nm (solvent included), which is somewhat lower than the observed one (Table 2), 558 nm at low concentration. Different DFT functionals and more extended basis sets have been used, without improving the agreement between theory and experimental results (results in the SI). Again, this could indicate that the emitting species are not under a monomeric form.

$[Au\{\mu\text{-}Se_2P(OEt)_2\}]_2$ (2). We analyze now the structural properties of the $[Au]_{2n}$ (n = 1, 8) species, derived from compound **2**, in which the Au−Au distance is shorter than in **4**, and consequently expected to be the subject of a strong aurophilic interaction. The optimized geometries of $[Au]_2$ and $[Au]_4$ are shown in Figure 4, and relevant computed metrical data are reported in Table 4. The MP2 optimized geometries are in excellent agreement with the X-ray data, reminding us that the species exists under a polymeric form in the crystal.[6] This is particularly noteworthy for the $[Au]_4$ dimer in which both types of Au−Au distances (intra- and intermonomers) are nicely reproduced by the calculations. As is well-known, this post-Hartree−Fock technique takes into account nondynamical correlation and consequently provides a better description of the long-range interactions which are involved in the Au···Au aurophilic interaction. It is worth noting that the Au1a−Au1b distance computed for $[Au]_2$ (2.886 Å) is smaller than the corresponding experimental value (2.946 Å) observed in the X-ray structure of the $[Au\{\mu\text{-}Se_2P(OEt)_2\}]_2$ polymer.[6] Such underestimation of the Au···Au distance by MP2 computations has also been noted in the case of complex **4** (*vide supra*).

Table 4. Comparison of the Optimized Geometries of $[Au]_2$ and $[Au]_4$ with the X-Ray Structure of 2 (Distances Are in Ångstroms and Angles in Degrees)

species		X-ray[a]	PBE0	MP2
$[Au]_2$	Au1a−Au1b	2.943	3.044	2.886
	Au1a−Se1a	2.409	2.459	2.453
	Se1b−P	2.177	2.216	2.200
	Se1b−Au1b−Se1b′	169	171	169
	Se1a−Au1a−Se1a′	176	180	179
	Se1a−P−Se2a	118	119	118
	Se1a−Au1a−Au1b−Se1b	−44	−49	−44
$[Au]_4$	Au1a−Au1b	2.943	3.067	2.943
	Au1b−Au2a	3.033	3.117	3.034
	Au1a−Au1b−Au2a	180	180	179

[a]From ref 6.

Nevertheless, the intramonomer Au1a−Au1b distance remains shorter than the Au1b−Au2a intermonomer one.

As can be seen in Table 4, the PBE0 computed optimized geometries for $[Au]_2$ and $[Au]_4$ exhibit a slight overestimation of bond lengths relative to the X-ray data, especially regarding the Au−Au distance (3−4%). We note the satisfying agreement for the bond angles. The fact that in $[Au]_4$ the intramonomer Au1a−Au1b distance is shorter than the intermonomer Au1b−Au2a distance is also correctly reproduced. Indeed, the computed difference (0.05 Å) is close to the observed one (0.09 Å).

As said above, the aurophilic interaction, which is mainly responsible for the observed short Au−Au distances, is not properly described using standard DFT computations as exemplified by the DFT overestimation of the Au−Au distances. Concomitantly, the DFT computed binding energy between two $[Au]_2$ units within the $[Au]_4$ species, taking into account the BSSE (basis set superposition error) and the solvent (THF) effect, is found equal to 4.2 kcal/mol, much lower than the generally accepted value for the aurophilic interaction energy, i.e., ca. 9 kcal/mol.[3b] Under the same conditions of computations, the MP2 computed binding energy is found equal to 11.2 kcal/mol. The overestimation of the Au−Au distance is also present and more accentuated in the DFT optimized $[Au]_6$ oligomer (not shown here), with averaged intra- and intermomomer Au−Au distances of 3.098 Å and 3.329 Å, respectively. Finally, it is worth noting that the vibration frequency analysis for the $[Au]_2$ and $[Au]_4$, which has been carried out at the DFT level, led us to a very good agreement for the Au−Se stretching mode, i.e., 227 cm^{-1} (computed) vs 235 cm^{-1} (observed).[6] Thus, although the Au−Au distance is overestimated, other structural properties are correctly depicted, using PBE0 computations, and one may anticipate the spectroscopic properties to be correctly described at the TDDFT level. On the other hand, using sophisticated post-HF techniques, such as CASPT2 or MRCI, is not possible for the investigated oligomers, due to their excessive demand of computational time.

We consider now the excitation spectrum of the $[Au\{\mu\text{-}Se_2P(OEt)_2\}]_2$ species. Experimentally, two distinct bands are observed at respectively 361 and 418 nm (7.4×10^{-3} M concentration in 2-MeTHF solvent).[6] Moreover, it must be pointed out that the recorded absorption spectrum, under the same experimental conditions, is rather flat and structureless, suggesting the presence of different gold species in solution, probably different oligomers, which cannot be distinguished experimentally. Therefore, TDDFT calculations have been carried out on $[Au]_{2n}$ oligomers of various lengths (n = 1−8). Since DFT optimizations of the largest oligomers would be too demanding computationally and anyway do not reproduce accurately enough the interaction between monomers, we have used structures taken out of the X-ray structure of **2** which contains regular linear infinite chains of identical $[Au]_2$ monomers.[6] Nevertheless, the DFT optimized geometries for the monomer and the dimer being available (see above), TDDFT computations have also been carried out using these geometries for comparison. In Table 5 are given the computed excitation wavelengths (λ in nm), the oscillator strengths (f), and the corresponding electron transitions with their weights (%) in the excitation. One can notice the small difference between the computed wavelengths using either optimized or X-ray geometries. This indicates that the influence of the Au−Au distance on the electronic spectra is not critical. Moreover,

Table 5. Computed HOMO−LUMO Gaps and Electronic Transitions of Lowest Energy (Values in Parentheses Are Computed Considering Solvent THF)

			X-ray-generated geometry (see text)		
	HOMO−LUMO gap (eV)	PBE0 optimized geometry λ (nm)	λ (nm)	f	electronic transitions (weight)
$[Au]_2$	4.74/4.85[a]	346 (338)	333 (325)	0.011	HOMO → LUMO (95%)
		276 (278)	257 (260)	0.200	HOMO−2 → LUMO+1 (46%)
					HOMO−1 → LUMO+2 (32%)
$[Au]_4$	4.27/4.20[a]	368	378	0.100	HOMO → LUMO (86%)
		305	300	0.102	HOMO → LUMO+3 (86%)
$[Au]_6$	3.93		394	0.177	HOMO → LUMO (50%)
					HOMO−1 → LUMO (30%)
			326	0.232	HOMO → LUMO+4 (71%)
$[Au]_8$	3.75		405	0.801	HOMO → LUMO (82%)
			336	0.121	HOMO →LUMO+5 (59%)
$[Au]_{10}$	3.66		416	1.245	HOMO → LUMO (79%)
			343	0.260	HOMO → LUMO+6 (30%)
$[Au]_{12}$	3.59		422	1.701	HOMO → LUMO (73%)
$[Au]_{14}$	3.54		426	2.165	HOMO → LUMO (65%)
					HOMO → LUMO+1 (13%)
$[Au]_{16}$	3.48		429	2.646	HOMO → LUMO (55%)
					HOMO → LUMO+1 (19%)

[a]First value, from the PBE0 optimized geometry; second value, from the X-ray-generated geometry.

calculations including solvent corrections have little effect on the computed wavelengths, as can be seen for the $[Au]_2$ and $[Au]_4$ cases.

First of all, it is worth noting that the computed wavelengths for the $[Au]_2$ unit (333 and 257 nm) disagree with the observed excitation wavelengths (418 and 361 nm). This disagreement is independent from the choice of the used geometry (X-ray or optimized) or of the consideration or not of the solvent effect. This result seems to indicate that the species responsible for the excitation spectrum are not $[Au]_2$ units. We remind the reader that for complex **4** the TDDFT computed electronic spectrum agrees with experimental results. The same discrepancy holds for the $[Au]_4$ oligomer. On the other hand, when lengthening the polymer chain, i.e., when going from $[Au]_2$ to $[Au]_{16}$, the computed wavelengths increase (in accordance with the diminution of the HOMO−LUMO gap, see Table 5) and converge to values closen to the observed ones. This is shown in Figure 6, where the asymptotic limits of the computed wavelengths are about 430 and 360 nm (gas phase), close to the experimental ones, i.e., 418 and 361 nm. It is also worth noting that the oscillator strength increases with the lengthening of the oligomeric chain. This result will be explained later in the text. Thus, it can be concluded that the observed excitation spectrum is the response of a polymer and not the result of absorptions of independent $[Au]_2$ monomers, or of small oligomers. The same trend is found when computing the electronic spectra of $[Au\{\mu\text{-}Se_2P(O^iPr)_2\}]_{2n}$ oligomers, where the isopropyl group replaces the ethyl one, i.e., that the computed excitation wavelengths using TDDFT increase with the lengthening of the polymeric chain. Indeed, the following values, 330, 371, 398, and 406 nm, have been obtained for the highest excitation wavelength for respectively n = 1, 2, 3, and 4.

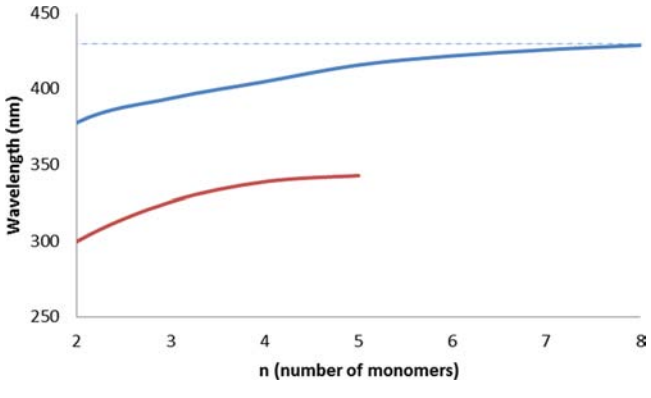

Figure 6. Computed optical absorption wavelengths vs n in the $[Au]_{2n}$ oligomers (upper curve for the highest excitation wavelength).

In order to confirm our analysis, we used two methods to measure the aggregate size of $[Au_2\{Se_2P(OEt)_2\}_2]$ species in solution. One is based on ElectroSpray Ionization-Mass Spectrometer (ESI-MS) molecular weight measurements and the second one, on Vapor Pressure Osmometry (VPO). Contrarily to ESI-MS, the latter technique did not enable us to carry out molecular weight measurements; this is likely to be due to the intrinsic, volatile nature of the gold(I) compounds under consideration.

While little information about aggregation was observed from the ESI-MS spectra of $[Au_2\{\mu\text{-}Se_2P(OEt)_2\}_2]$ in dilute solution ~2×10^{-4} M, three bands centered at 2874.2, 3821.4, and 4770.0 do correspond approximately to the trimer ($[Au_2\{\mu\text{-}Se_2P(OEt)_2\}_2]_3$; M_{calcd} = 2867.05), tetramer ($[Au_2\{\mu\text{-}Se_2P(OEt)_2\}_2]_4$; M_{calcd} = 3822.73), and pentamer ($[Au_2\{\mu\text{-}Se_2P(OEt)_2\}_2]_5$; M_{calcd} = 4778.41), respectively, at a concentration of ~2×10^{-2} M (SI Figure S6). Due to the detection limits, peaks corresponding to molecular weights larger than 5000 could not be clearly detected. Thus, the molecular aggregation expected on the basis of the analysis of the excitation spectra is clearly confirmed by our ESI-MS experiments.

In order to provide an assignment of the observed excitation bands, let us consider the electronic structure of the species under consideration. We observe that the excitation of lower energy corresponds mainly to a HOMO−LUMO transition, whatever the considered oligomer is (Table 5). The

dx.doi.org/10.1021/ic301763k | Inorg. Chem. 2012, 51, 11851−11859

Table 6. HOMO, LUMO, and LUMO+n+1 Composition of the $[Au]_{2n}$ Oligomers (in %) in the Following Order: Au(5d,6s,6p)/Se/P (X-Ray Generated Geometries)

species	$[Au]_2$	$[Au]_4$	$[Au]_6$	$[Au]_8$
LUMO+n+1	53(2,38,13)/20/21	50(5,43,2)/24/21	49(6,32,11)/29/18	46(5,28,14)/32/18
LUMO	36(4,9,23)/47/15	40(3,5,32)/42/14	48(3,6,38)/38/12	48(3,6,39)/38/12
HOMO	33(18,14,1)/64/1	48(31,16,1)/49/1	58(40,16,2)/39/1	59(40,17,2)/39/1

participation of the different atoms and of gold valence orbitals (AO) within these frontier MOs is given in Table 6.

The frontier orbitals of $[Au]_2$ (Figure in SI) are quite similar to those of complex **4**, except that its HOMO has a larger gold contribution (33%) and a lower selenium contribution (64%). This may be related to the strong aurophilic interaction in **2**, as compared to **4**.

So, the HOMO and LUMO of $[Au]_2$ involve predominantly gold and selenium and, to a lesser extent, phosphorus for the LUMO. The excitation corresponding to the first band exhibits a significant electron transfer from selenium to phosphorus atoms since the weight of gold atoms is almost the same in these frontier MOs. Focusing now on the gold valence AO participations to the HOMO and LUMO, the weight of the 5d orbitals drops drastically when passing from the HOMO to the LUMO, i.e., 18% vs 4%, whereas the weight of the 6p orbitals increases sharply from 1% to 23%. This means that the HOMO−LUMO transition exhibits also a gold metal centered character. This metal-centered charge transfer is larger in $[Au]_2$ than in complex **4**, due to the larger gold participation in the HOMO of $[Au]_2$.

Relevant frontier orbitals of the $[Au]_4$ dimer are shown in Figure 7, whereas those of $[Au]_6$ are given in the Supporting Information (SI).

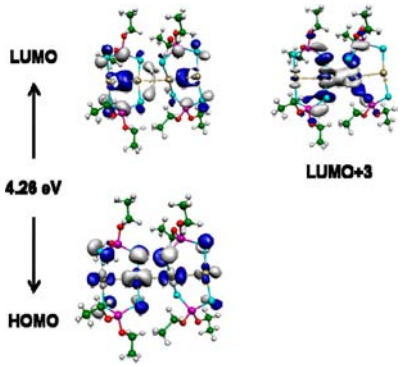

Figure 7. Plots (cutoff equal to 0.035 au) of the HOMO and LUMO (left) and LUMO+3 (right) of the $[Au]_4$ model.

They look approximately as constituted by doubling those of the $[Au]_2$ MOs. However, the relative contributions of gold and selenium in these MOs (see Table 6) are noticeably different from those of $[Au]_2$. In the HOMO, the gold participation increases to 48%, to the disadvantage of selenium (49%). As in the monomers **4** and $[Au]_2$, this HOMO is a combination of Se lone pairs with the fully antibonding combination of $5d_{z^2}$ gold AOs. With three antibonding contacts, this $5d_{z^2}$ combination is more antibonding in $[Au]_4$ than in $[Au]_2$. It is therefore higher in energy and mixes to a larger extent with the Se lone pairs in the HOMO. For symmetrical reasons, the LUMO of $[Au]_4$, which has a fully 6p bonding character, has also a somehow larger gold participation (40%) than in $[Au]_2$. As discussed above, it has stronger bonding character on the intramolecular Au−Au contacts. The increase in the metal participation in the HOMO and LUMO is expected to continue with increasing n, up to an asymptotical value approaching the infinite polymer situation. This limit is actually reached for n = 8, with a maximum of gold participation in both the HOMO (59%, mainly 5d) and the LUMO (48%, mainly 6p; see Table 6). Whatever the oligomer length is, i.e., n > 1, the HOMO−LUMO transition is mainly a 5d to 6p gold-centered transition (as already claimed by different authors[6,19,22]) together with a gold to phosphorus transition since the participation of selenium is almost the same in these frontier MOs. This assignment is consistent with the fact that the oscillator strength of this excitation increases with the number of gold atoms of the oligomers. More than that, starting from $[Au]_8$, this property varies linearly with the gold atom number. At this point of the discussion, it is worth reminding the reader that the nature of the HOMO−LUMO transition is different for the large $[Au]_{2n}$ oligomers as compared to the $[Au]_2$ monomer (occurrence of a selenium to phosphorus charge transfer).

The transition of higher energy (Table 5) is due in all cases to an electronic transition from the HOMO to the LUMO+n+1. It turns out that these unoccupied MOs can be described as being the fully bonding combination of the monomeric 6s-containing orbital described at the beginning of this section. It is primarily bonding between the $[Au]_2$ units, as exemplified by the LUMO+3 of $[Au]_4$ shown in Figure 7.

These LUMO+n+1 orbitals exhibit a similar composition for the larger oligomers. In the case of $[Au]_8$, the following MO composition of LUMO+5 is obtained: gold (47%), selenium (32%), and phosphorus (18%). Thus, the HOMO to LUMO+5 transition responsible for the spectrum short wavelength of $[Au]_8$ exhibits the same feature as the HOMO−LUMO one, i.e., mainly a charge transfer from gold to phosphorus, together with a 5d to 6s gold centered transition. Contrarily to the transition of lower energy, its oscillator strength is moderate and does not depend on the number of gold atoms. This is due to the fact that the 5d → 6s transition is forbidden.

4-. CONCLUSION

The structure and optical properties of several polynuclear gold(I) species, namely the diselenophosphate complexes **1**, **2**, **3**, and **4** $[Au\{\mu\text{-}Se_2P(CH_2)_2Ph)_2\}]_2$ (Scheme 1), exhibiting interesting structural, absorption, and emission properties have been studied. Whereas **1** and **2** have been previously reported,[6] the synthesis, full characterization, and optical properties of **3** and **4** are described in this paper. In the solid state, **1**, **2**, and **3** give polymers, whereas **4** exists under a dinuclear monomeric form. The absorption and phosphorescence properties of **4** have been rationalized using DFT and TDDFT computations. In particular, Au−Au bonding seems to appear in its first singlet and triplet states, whereas such a bond does not exist in the ground state. Then, the structure and optical properties of **2** were investigated. The X-ray study brings to light its polymeric structure and the occurrence of short Au···Au distances due to significant aurophilic interaction. The observed short Au···Au

distances are reproduced using MP2 computations, whereas they are overestimated by DFT calculations. The influence of polymerization, through aurophilic bonding, on the optical properties of such species is analyzed. TDDFT calculations show that the observed UV−visible excitation spectrum is the response of high oligomers and not of monomers or low oligomers. The existence of such oligomers of **2** in solution is confirmed by ESI-MS measurements. An assignment of the observed bands of **2** is proposed. The excitation corresponding to the highest observed wavelength band, which is mainly a HOMO to LUMO transition, exhibits a composite character, electron density transfer from gold to phosphorus atoms, and metal centered 5d to 6p transition.

■ ASSOCIATED CONTENT

Supporting Information

DFT optimized cartesian coordinates; MP2 optimized cartesian coordinates; Cartesian coordinates from the $[Au_2\{Se_2P(OEth_2)_2\}_2]$ RX model PBE1PBE/LANL2DZ + polarization + diffuse on Au; distances benchmark in function of the functional; computed emission wavelength in function of the basis set; TD-DFT benchmark; frontier MO diagrams of $[Au]_2$, $[Au]_4$, and $[Au]_6$; plots of the HOMO and LUMO of $[Au]_2$ model; CIF files of 3 and 4; and ESI_MS_data. This material is available free of charge via the Internet at http://pubs.acs.org.

■ AUTHOR INFORMATION

Corresponding Author

*E-mail: abdou.boucekkine@univ-rennes1.fr; saillard@univ-rennes1.fr; chenwei@mail.ndhu.edu.tw.

Notes

The authors declare no competing financial interest.

■ ACKNOWLEDGMENTS

Financial support from the National Science Council of Taiwan (CWL) is gratefully acknowledged. We thank Dr. Mitch Chiang in Academia Sinica for acquisition of the ESI-mass spectra. The authors are grateful to GENCI-IDRIS and GENCI-CINES for an allocation of computing time (Grant No. 2011-080649). J.-Y.S. thanks the IUF for support.

■ REFERENCES

(1) (a) *Modern Supramolecular Gold Chemistry: Gold-Metal Interactions and Applications*; Laguna, A., Ed.; Wiley-VCH: Weinheim, Germany, 2008. (b) *Gold Chemistry: Applications and Future Directions in the Life Sciences*; Mohr, F., Ed.; Wiley-VCH: Weinheim, Germany, 2009. (c) Yam, V. V.-W.; Cheng, E. C. C. *Chem. Soc. Rev.* **2008**, *37*, 1806−1813.

(2) Schmidbaur, H.; Schier, A. *Chem. Soc. Rev.* **2008**, *37*, 1931−1951.

(3) (a) Pyykko, P. *Chem. Soc. Rev.* **2008**, *37*, 967−1997. (b) Pyykkö, P. *Angew. Chem., Int. Ed. Engl.* **2004**, *43*, 4412−4456.

(4) (a) Elbjeirami, O.; Gonser, M.W. A.; Stewart, B. N.; Bruce, A. E.; Bruce, M. R. M.; Cundari, T. R.; Omary, M. A. *Dalton Trans.* **2009**, 1522−1533. (b) Muñiz, J.; Sansores, L. E.; Martinez, A.; Salcedo, R. *J. Mol. Struct.: THEOCHEM* **2007**, *820*, 141−147. (c) Crespo, O.; Diez-Gil, C.; Laguna, A.; Monge, M.; Gimeno, M. C; Ospino, I. *Dalton Trans.* **2011**, *40*, 10038−10046. (d) Sansores, L. E.; Salcedo, R.; Martínez, A. *J. Mol. Struct.: THEOCHEM* **2004**, *677*, 145−151. (e) Mendizabal, F.; Reyes, D.; Olea-Azar, C. *Int. J. Quantum Chem.* **2006**, *106*, 906−912. (f) Van Zyl, W. E.; Lopez-de-Luzuriaga, J. M.; Mohamed, A. A.; Staples, R. J.; Fackler, J. P., Jr. *Inorg. Chem.* **2002**, *41*, 4579−4589. (g) Azani, M.-R.; Castillo, O.; Gallego, M. L.; Parella, T.; Aullon, G.; Crespo, O.; Laguna, A.; Alvarez, S.; Mas-Ballesté, R.; Zamora, F. *Chem.—Eur. J.* **2012**, *18*, 9965−9976. (h) Hemmert, C.; Poteau, R.; Jean-Baptiste dit Dominique, F.; Ceroni, P.; Bergamini, G.; Gornitzka, H. *Eur. J. Inorg. Chem.* **2012**, 3892−3898.

(5) Rawashdeh-Omary, M. A.; Omary, M. A.; Patterson, H. H.; Fackler, J. P., Jr. *J. Am. Chem. Soc.* **2001**, *123*, 11237−11247.

(6) You, H.-J.; Fang, C.-S.; Lin, J.-L.; Sun, S.-S.; Liu, C.-W. *Inorg. Chem.* **2010**, *49*, 7641−7643.

(7) Perrin, D. D.; Armarego, W. L. F.; Perrin, D. R. *Purification of Laboratory Chemicals*, 2nd ed.; Pergamon Press: Oxford, U. K., 1980.

(8) (a) Sarkar, B.; Fang, C.-S.; Yu, L.-Y.; Wang, J.-C.; Liu, C. W. *New J. Chem.* **2009**, *33*, 626−633. (b) Artem'ev, A. V.; Malysheva, S. F.; Gusarova, N. K.; Trofimov, B. A. *SYNTHESIS* **2010**, *11*, 1777−1780.

(9) *SMART V4.043: Software for the CCD Detector System*; Bruker Analytical X-ray System: Madison, WI, 1995.

(10) *SAINT V4.043: Software for the CCD Detector System*; Bruker Analytical X-ray System: Madison, WI, 1995.

(11) Sheldrick, G. M. *SADABS*; University of Gottingen: Gottingen, Germany, 1996.

(12) *SHELXL 5.10 (PC Version): Program Library for Structure Solution and Molecular Graphics*; Bruker Analytical X-ray System: Madison, WI, 1997.

(13) (a) Adamo, C.; Barone, V. *J. Chem. Phys.* **1999**, *110*, 6158−6170. (b) Ernzerhof, M.; Scuseria, G. E. *J. Chem. Phys.* **1999**, *110*, 5029−5036.

(14) Hay, P. J.; Wadt, W. R. *J. Chem. Phys.* **1985**, *82*, 270−283, ibid. 299−310.

(15) Tomasi, J.; Mennucci, B.; Cammi, R. *Chem. Rev.* **2005**, *105*, 2999−3094.

(16) Frisch, M. J.; et al. *Gaussian 09*, revision A.02; Gaussian Inc.: Wallingford, CT, 2009.

(17) Flükiger, P.; Lüthi, H. P.; Portmann, S.; Weber, J. *Molekel 4.3*; Swiss Center for Scientific Computing: Manno, Switzerland, 2000−2002. http://www.cscs.ch/molkel/ (accessed Oct. 2012).

(18) (a) Gorelsky, S. I. *AOMix: Program for Molecular Orbital Analysis*; University of Ottawa: Ottawa, Canada, 2009. http://www.sg-chem.net/ (accessed Oct. 2012). (b) Gorelsky, S. I.; Lever, A. B. P. *J. Organomet. Chem.* **2001**, *635*, 187−196.

(19) Huang, S.-P.; Kanatzidis, M. G. *Inorg. Chem.* **1991**, *30*, 3572−3575.

(20) Dibrov, S. M.; Ibers, J. A. *Chem. Commun.* **2003**, 2158−2159.

(21) (a) Baron, M.; Tubaro, C.; Biffis, A.; Basato, M.; Graiff, C.; Poater, A.; Cavallo, L.; Armaroli, N.; Accorsi, G. *Inorg. Chem.* **2012**, *51*, 1778−1784. (b) King, C.; Wang, J.-C.; Khan, M. N. I.; Fackler, J. P., Jr. *Inorg. Chem.* **1989**, *28*, 2145−2149.

(22) Lee, Y.-A.; McGarrath, J. E.; Lachicotte, R. J.; Eisenberg, R. *J. Am. Chem. Soc.* **2002**, *124*, 10662−10663.